Topological insulators and metal-insulator transition in the pyrochlore iridates

Bohm-Jung Yang[1] and Yong Baek Kim[1,2]

[1]*Department of Physics, University of Toronto, Toronto, Ontario, Canada M5S 1A7*

[2]*School of Physics, Korea Institute for Advanced Study, Seoul 130-722, Korea*

The possible existence of topological insulators in cubic pyrochlore iridates $A_2Ir_2O_7$ (A = Y or rare-earth elements) is investigated by taking into account the strong spin-orbit coupling and trigonal crystal-field effect. It is found that the trigonal crystal-field effect, which is always present in real systems, may destabilize the topological insulator proposed for the ideal cubic crystal field, leading to a metallic ground state. Thus the trigonal crystal field is an important control parameter for the metal-insulator changeover. We propose that this could be one of the reasons why distinct low-temperature ground states may arise for the pyrochlore iridates with different A-site ions. On the other hand, examining the electron-lattice coupling, we find that softening of the $\mathbf{q}$ = 0 modes corresponding to trigonal or tetragonal distortions of the Ir pyrochlore lattice leads to the resurrection of the strong topological insulator. Thus, in principle, a finite-temperature transition to a low-temperature topological insulator can occur via structural changes. We also suggest that the application of the external pressure along [111] or its equivalent directions would be the most efficient way of generating strong topological insulators in pyrochlore iridates.

I. INTRODUCTION

Topological band insulators arise from nontrivial Berry phase of electron wave functions and possess gapless boundary states as a consequence of topological properties of the bulk electron energy bands.[1–12] Topological invariants of electron wave functions in such topological insulators can be used to describe/identify two-dimensional quantum spin-Hall insulators and three-dimensional strong topological insulators. The presence of the gapless boundary states and the associated topological properties have recently been confirmed by a series of remarkable experiments on HgCdTe, $Bi_{1-x}Sb_x$, Bi_2Se_3, Bi_2Te_3, and other materials.[13–18] It has been known that the strong spin-orbit coupling in these systems provides an essential ingredient for the nontrivial Berry phase of electron wave functions. One important future direction is to understand the effect of interactions on the topological insulators. Growing interests on combined effects of electron correlation and topological properties have naturally lead to recent fascinating studies on the realization of topological phases in transition-metal oxides with d electrons,[19,20] instead of more conventional s- or p-orbital systems where electron correlation is less important.

Transition-metal oxides with $5d$ electrons are characterized by the strong spin-orbit coupling due to the large atomic number of $5d$ transition-metal elements. As a result, the spin-orbit coupling competes with the kinetic and interaction energies, leading to substantial correlation effects despite the relatively extended nature of the $5d$ orbitals. This feature, for example, is confirmed by recent experiments on Sr_2IrO_4,[21–24] where the spin-orbit coupling plays an essential role in the formation of the Mott-insulator ground state. In the case of the so-called hyperkagome material $Na_4Ir_3O_8$, a spin-liquid ground state is proposed, manifesting strong correlation effects in $5d$ electron systems.[25–32] Moreover iridium oxides are considered as promising candidate systems where we can study the interplay between electron correlation and strong spin-orbit coupling. Perhaps most interestingly, the iridium oxides may also be ideal materials for the occurrence of topological insulators. It is suggested that the honeycomb lattice of Ir ions in Na_2IrO_3 with the complex hopping amplitudes arising from the strong spin-orbit coupling may lead to a quantum spin-Hall insulator.[19] Three-dimensional pyrochlore lattice of Ir with the structure described in Fig. 1 is also suggested as a candidate system for a strong topological insulator.[20] The possibility of the topological Mott insulators where the spinons, not the electrons, possess topological band structures is discussed as a result of correlation effects.[20,33]

In this work, we study the possibility and stability of strong topological insulators in pyrochlore iridates, $A_2Ir_2O_7$ (A = Y or rare-earth elements) by taking into account both of the strong spin-orbit coupling and trigonal crystal-field effect induced by a local distortion of IrO_6 octahedra. Due to the extended nature of $5d$ electron wave functions, the local
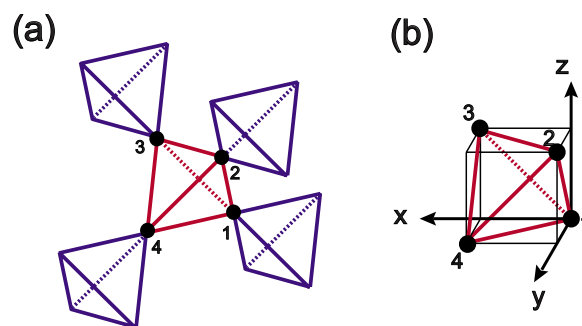

FIG. 1. (Color online) (a) Structure of the pyrochlore lattice. An Ir atom sits at each vertex of a tetrahedron. Four sites within a tetrahedral unit cell are numbered from 1 to 4. (b) The coordinate system used in this paper.

crystal-field strength in $5d$ systems also becomes a large energy scale competing with electron interaction and spin-orbit coupling.[34] The strength of the trigonal crystal-field effect may be different for distinct choices of the A-site ion in $A_2Ir_2O_7$. Given that there exist a variety of choices for the A site, the pyrochlore iridates offer the opportunity to control the relative strength of the crystal-field effect and the spin-orbit coupling. In addition, the pyrochlore iridates show both metallic and insulating ground states at low temperatures as well as finite-temperature metal-insulator transitions depending on the A-site ions.[35–37] Thus it would be very interesting to understand the origin of distinct phases and phase transitions.

Here we derive an effective Hamiltonian for the Ir ions in the pyrochlore iridates by carefully incorporating the trigonal crystal-field effect and using the appropriate spin-orbital basis. Previously an effective Hamiltonian was derived by Pesin and Balents[20] for the Ir ions in a perfect octahedral environment with the cubic O_h symmetry and it was found that the Ir pyrochlore system supports a strong topological insulator when the strength of spin-orbit coupling is sufficiently large. In contrast we find that the trigonal crystal-field effect, which is always present in real pyrochlore systems, is quite significant and it can lead to a metallic ground state.

On the other hand, we find that the distortions of the Ir pyrochlore lattice induced by softening of certain $\mathbf{q}=0$ phonon modes give rise to the resurrection of strong topological insulators. This suggests that finite-temperature metal-insulator transition can occur through structural distortions such that the low-temperature ground state is a strong topological insulator. It is interesting to notice that recent experiments on $Sm_2Ir_2O_7$ and $Eu_2Ir_2O_7$ show structural changes at the metal-insulator transition even though the low-temperature ground state seems to be magnetic and show spin-glasslike behavior.[38,39] We also suggest from the studies of the electron-lattice coupling that applying pressure along [111] or its equivalent directions would be the most efficient way of generating strong topological insulators in pyrochlore iridates.

The rest of the paper is organized as follows. In Sec. II we derive the effective hopping Hamiltonian including the trigonal crystal-field effect. We first consider the influence of local trigonal distortion of the oxygen octahedra on Ir t_{2g} electrons. Then we explain the derivation of the corresponding lattice Hamiltonian. In Sec. III, the evolution of the electronic structure induced by trigonal crystal field in the presence of the strong spin-orbit coupling is described in detail. Here we explain how a metallic state may arise when the trigonal crystal-field effect is present. In Sec. IV, we discuss the effect of electron-lattice coupling on the electronic structure of the Ir pyrochlore system. We show how the electron-lattice coupling can lead to strong topological insulators. Finally, we conclude in Sec. V. The detailed expressions for various matrices describing the effective Hamiltonian are given in the Appendix.

II. EFFECTIVE HOPPING HAMILTONIAN WITH TRIGONAL CRYSTAL FIELD

In this section we investigate the effect of local trigonal crystal field on the electronic structure of Ir $5d$ electrons. In
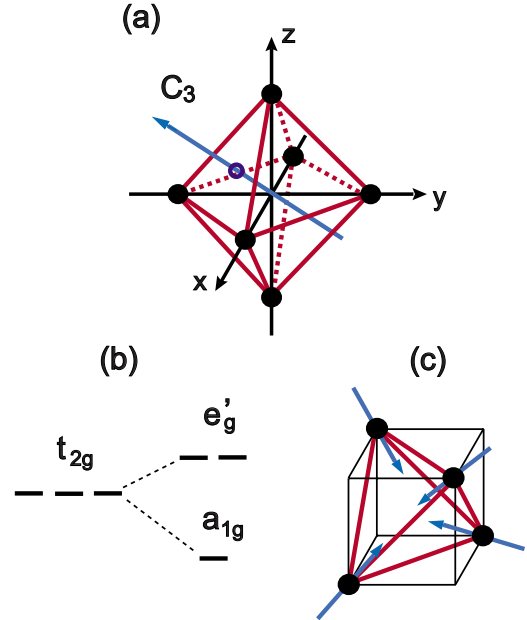

FIG. 2. (Color online) Trigonal crystal field around an Ir^{4+} ion. (a) Local geometry of an IrO_6 octahedron. A trigonal distortion is induced by compression or elongation of the surrounding oxygen octahedron along a C_3 symmetry axis for threefold rotation. (b) Splitting of degenerate t_{2g} states under the trigonal crystal field. (c) Local C_3 axes for four Ir ions constituting a tetrahedron; each C_3 axis points to the body center of the tetrahedron.

Sec. II A we explain the degeneracy lifting of t_{2g} orbitals under trigonal crystal fields. The effective hopping Hamiltonian including the trigonal crystal field is derived in Sec. II B. Detailed procedures of the derivation can be found there, as well.

A. Trigonal crystal field

Each Ir^{4+} ion is coordinated by six oxygen anions which are at equal distance from the central Ir^{4+} cation. The actual coordinates of the surrounding oxygen anions have a free positional parameter, so called the oxygen x parameter, which depends on material properties. In general, the six oxygen ions around a central Ir^{4+} form a distorted octahedron where the amount of distortion can be parametrized by the oxygen x parameter.[40,41] For $x=x_c=5/16$, each Ir^{4+} ion is under a perfect local cubic crystal field. The deviation of x from the ideal value of x_c generates a trigonal crystal field. The trigonal distortion of an oxygen octahedron is accompanied by compression $(x>x_c)$ or elongation $(x<x_c)$ of the oxygen octahedron along one of the C_3 symmetry axis for threefold rotation. A local geometry of an IrO_6 octahedron and a C_3 symmetry axis for the trigonal distortion are described in Fig. 2(a).

Under the trigonal distortion, the local symmetry group around an Ir site reduces from the cubic O_h to D_{3d}. Due to the trigonal crystal field, degenerate t_{2g} orbitals split into a singlet a_{1g} state and a doublet e'_g state belonging to A_{1g} and

E_g irreducible representations of the D_{3d} point group, respectively [see Fig. 2(b)]. A C_3 symmetry axis corresponds to one of the [111] or its equivalent axes. Taking the local $[n_1 n_2 n_3]$ directions as the C_3 symmetry axes ($n_i = \pm 1$), the effect of trigonal crystal field on t_{2g} states can be described by the following Hamiltonian:

$$H_{\mathrm{tri}} = -\frac{\Delta_{\mathrm{tri}}}{3} \begin{pmatrix} 0 & n_1 n_2 & n_1 n_3 \\ n_1 n_2 & 0 & n_2 n_3 \\ n_1 n_3 & n_2 n_3 & 0 \end{pmatrix}.$$

Here we have chosen a local basis as $\Psi^{\dagger} = (d_{yz}^{\dagger}, d_{zx}^{\dagger}, d_{xy}^{\dagger})$. The singlet a_{1g} state with the energy $E_a = -2\Delta_{\mathrm{tri}}/3$ is given by

$$|a_1\rangle \equiv a_1^{\dagger}|0\rangle = \frac{1}{\sqrt{3}}[n_1|d_{yz}\rangle + n_2|d_{zx}\rangle + n_3|d_{xy}\rangle]. \tag{1}$$

The eigenvectors for the e_g' doublet states with the energy $E_e = \Delta_{\mathrm{tri}}/3$ can be written as

$$|e_+\rangle \equiv e_+^{\dagger}|0\rangle = \frac{1}{\sqrt{3}}[n_1\omega|d_{yz}\rangle + n_2\omega^2|d_{zx}\rangle + n_3|d_{xy}\rangle],$$

$$|e_-\rangle \equiv e_-^{\dagger}|0\rangle = \frac{1}{\sqrt{3}}[n_1\omega^2|d_{yz}\rangle + n_2\omega|d_{zx}\rangle + n_3|d_{xy}\rangle], \tag{2}$$

where $\omega = e^{i(2\pi/3)}$.

In Fig. 2(c), we show the local C_3 axes of the four Ir sites constituting a tetrahedral unit cell. Each C_3 axis points to the body center of the tetrahedron. Considering the trigonal distortions of IrO$_6$ octahedra and their relative orientations, we construct the effective hopping Hamiltonian for Ir d electrons on the pyrochlore lattice. The resulting Hamiltonian is given by

$$H = \sum_{i,n,\alpha} (\varepsilon_\alpha - \mu) d_{in\alpha}^{\dagger} d_{in\alpha} + \sum_{\langle ij \rangle} \sum_{n,n'} \sum_{\alpha,\alpha'} \{ d_{in\alpha}^{\dagger} T_{n\alpha,n'\alpha'} d_{jn'\alpha'}$$

$$+ \text{H.c.}\}. \tag{3}$$

Here i and j are indices for unit cells while n and n' indicate Ir sites within a unit cell ($n = 1, 2, 3, 4$). We use the index α ($\alpha = 1, \ldots, 6$) to describe local spin-orbit eigenstates. Within the t_{2g} manifold, d electrons behave as if their effective orbital angular momentum is one with an additional minus sign.[20] Therefore, the effective total angular momentum of Ir d electrons, j_{eff} can be either 1/2 or 3/2. We use $\alpha = 1, 2$ to indicate the spin-orbit doublet with $j_{\mathrm{eff}} = 1/2$ and $\alpha = 3, 4, 5, 6$ to denote the spin-orbit quadruplet with $j_{\mathrm{eff}} = 3/2$. The on-site energy $\varepsilon_\alpha = \lambda_{SO}$ for the spin-orbit doublet and $\varepsilon_\alpha = -\lambda_{SO}/2$ for the spin-orbit quadruplet with the spin-orbit coupling strength given by λ_{SO}. $T_{n\alpha,n'\alpha'}$ is the hopping amplitudes between nearest-neighbor Ir sites and μ is the chemical potential.

In contrast to the tight-binding Hamiltonian derived by Pesin and Balents in Ref. 20 where a single energy scale t describes the hopping processes, the hopping amplitude $T_{n\alpha,n'\alpha'}$ has two independent parameters t_a and t_e in this case.
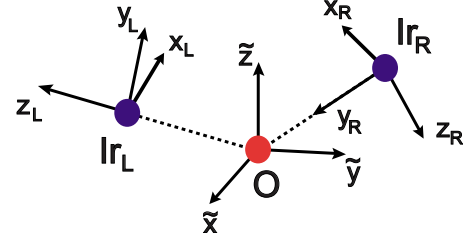

FIG. 3. (Color online) Local Ir-O-Ir configuration. Local octahedral axes for Ir atoms on the left-hand side (Ir$_L$) and the right-hand side (Ir$_R$) are not parallel to the global cubic axis adopted for the central oxygen atom.

These two hopping parameters come from the hopping processes between a_{1g} and e_{2g}' states under the trigonal crystal field, respectively. Under the perfect local cubic environment around an Ir site without a trigonal crystal field, $t_a = t_e$ is satisfied. In other words, the effect of trigonal crystal fields on the electronic structure can be captured by varying the relative magnitude of t_a/t_e. In the following section, we explain the procedures deriving the above effective Hamiltonian in Eq. (3).

B. Construction of the effective hopping Hamiltonian

We construct the effective Hamiltonian describing hopping processes between neighboring Ir t_{2g} orbitals through intermediating oxygen p orbitals in the following way. We first consider a small cluster composed of neighboring Ir-O-Ir atoms as shown in Fig. 3. Allowing Ir-O hopping processes, the three-atom cluster can be described by the following Hamiltonian:

$$H = H^{(0)} + H^{(1)}, \tag{4}$$

where

$$H^{(0)} = \eta_L^{\dagger} H_d^{(0)} \eta_L + \eta_R^{\dagger} H_d^{(0)} \eta_R + \tilde{p}^{\dagger} H_p^{(0)} \tilde{p} \tag{5}$$

and

$$H^{(1)} = \eta_L^{\dagger} V_L \tilde{p} + \tilde{p}^{\dagger} V_L^{\dagger} \eta_L + \eta_R^{\dagger} V_R \tilde{p} + \tilde{p}^{\dagger} V_R^{\dagger} \eta_R. \tag{6}$$

Here $H^{(0)}$ indicates on-site potentials at Ir and O sites while $H^{(1)}$ describes Ir-O hybridizations. The on-site atomic potentials of d and p orbitals give rise to the diagonal matrices, $H_d^{(0)} = \mathrm{diag}[E_a, E_e, E_e]$ and $H_p^{(0)} = \mathrm{diag}[E_p, E_p, E_p]$. Here E_a (E_e) is the atomic energy for an a_{1g} singlet (e_g' doublet) state composed of Ir d orbitals under the trigonal crystal field and E_p is the atomic energy of degenerate oxygen p orbitals. V_n ($n = L, R$) represents overlap integrals between Ir d orbitals and oxygen p orbitals. Taking into account the local trigonal crystal field of each Ir atom, we employ a basis, that is diagonal under the local trigonal crystal field, $\eta_n^{\dagger} = (a_{1,n}^{\dagger}, e_{+,n}^{\dagger}, e_{-,n}^{\dagger})$ to represent Ir t_{2g} orbitals. The subscript n indicates the locations of two Ir atoms on the left-hand side ($n = L$) or the right-hand side ($n = R$). $\tilde{p}^{\dagger} = (\tilde{p}_x^{\dagger}, \tilde{p}_y^{\dagger}, \tilde{p}_z^{\dagger})$ represents oxygen p orbitals connecting neighboring Ir atoms. It is important to notice that the local octahedral axes of Ir atoms are not parallel to the global cubic axes as described in Fig. 3. Each component of the oxygen p orbitals is defined with

respect to the global cubic axis while d orbital basis is defined with respect to the local octahedral coordinate of each Ir atom.

The effective hopping Hamiltonian between two neighboring Ir atoms is obtained from the second-order perturbation theory treating $H^{(1)}$ as a perturbation. The resulting Hamiltonian is given by

$$H_{L,R} = -\frac{1}{2}\eta_L^\dagger \left\{ \frac{1}{H_p^{(0)} - H_d^{(0)}} V_L V_R^\dagger + V_L V_R^\dagger \frac{1}{H_p^{(0)} - H_d^{(0)}} \right\} \eta_R + \text{H.c.} \tag{7}$$

The information about the relative orientation between two local octahedral axes of neighboring Ir atoms is contained in V_L and V_R. To construct V_L and V_R, we follow the approach used by Pesin and Balents in Ref. 20. We first construct matrices describing hopping processes between Ir t_{2g} and O p orbitals. It is convenient to define components of oxygen p and Ir t_{2g} orbitals with respect to the same cubic axis. In this case the Ir-O hopping processes are strongly constrained by the symmetries of d and p orbitals. The hopping matrices connecting (p_x, p_y, p_z) orbitals to (d_{yz}, d_{zx}, d_{xy}) orbitals are given by[20]

$$\tau_x^\pm = \pm \alpha_{pd\pi} \begin{pmatrix} 0 & 0 & 0 \\ 0 & 0 & 1 \\ 0 & 1 & 0 \end{pmatrix},$$

$$\tau_y^\pm = \pm \alpha_{pd\pi} \begin{pmatrix} 0 & 0 & 1 \\ 0 & 0 & 0 \\ 1 & 0 & 0 \end{pmatrix},$$

$$\tau_z^\pm = \pm \alpha_{pd\pi} \begin{pmatrix} 0 & 1 & 0 \\ 1 & 0 & 0 \\ 0 & 0 & 0 \end{pmatrix}.$$

Here the subscript and superscript of the matrix τ indicate the location of an O atom with respect to the Ir atom. For example, τ_x^+ describes Ir-O hopping processes when an O atom sits on the positive x axis with the Ir atom sitting at the origin. $\alpha_{pd\pi}$ is the hopping integral between neighboring p and d orbitals.

Since the local octahedral axes of Ir atoms are not parallel, we introduce an additional matrix $R^{(i)}$ for each ith Ir atom, which rotates the global cubic axis to a local octahedral axis. Under the action of $R^{(i)}$, the $\tilde{p}_n(n=x,y,z)$ orbitals defined with respect to the global cubic axis transform as $p_{i,n}^\dagger = R_{mn}^{(i)} \tilde{p}_m^\dagger$. Here $p_{i,n}$ denotes a p orbital defined with respect to the local octahedral axis of the ith Ir atom. In addition, we introduce the matrix Ω that transforms (d_{yz}, d_{zx}, d_{xy}) to the trigonal basis (a_1, e_+, e_-) in the following way, $e_{i,n}^\dagger = \Omega_{nm} d_{i,m}^\dagger$. From Eqs. (1) and (2), Ω is obtained as

$$\Omega = \frac{1}{\sqrt{3}} \begin{pmatrix} n_1 & n_2 & n_3 \\ n_1\omega & n_2\omega^2 & n_3 \\ n_1\omega^2 & n_2\omega & n_3 \end{pmatrix}.$$

Now we can construct V_L and V_R explicitly, which are given by $V_L = \Omega^* \tau_{p(L)} R^{(L)\dagger}$ and $V_R = \Omega^* \tau_{p(R)} R^{(R)\dagger}$. Here the subscript $p(L)$ $[p(R)]$ of τ indicates the location of the intermediating oxygen atom with respect to the local octahedral axis of the Ir ion on the left-hand (right-hand) side.

The effective hopping Hamiltonian in Eq. (7) can be written compactly as

$$H_{L,R} = \frac{1}{2}\eta_L^\dagger \{T_{\text{hop}} V_L V_R^\dagger + V_L V_R^\dagger T_{\text{hop}}\} \eta_R + \text{H.c.}, \tag{8}$$

where $T_{\text{hop}} \equiv \text{diag}[t_a, t_e, t_e]$ with $t_a = \alpha_{pd\pi}^2/(E_a - E_p)$ and $t_e = \alpha_{pd\pi}^2/(E_e - E_p)$. In the above, we have replaced V_R (V_L) by $V_R/\alpha_{pd\pi}$ ($V_L/\alpha_{pd\pi}$) to make t_a and t_e have conventional forms for hopping amplitudes. Note that $t_a = t_e$ in the absence of the trigonal crystal-field effects because $E_a = E_e$ is satisfied in that case. The effect of local trigonal field splitting can be considered by changing the relative magnitude of t_a/t_e.

Up to now we have neglected spin degrees of freedom. Since the spin-orbit coupling is the largest energy scale of the problem, it is convenient to use the local spin-orbit eigenstates as a basis for the representation of the Hamiltonian. To project the Hamiltonian onto the local spin-orbit basis, we define rotation matrices $D^{(i)}$ acting on the spin space, which is nothing but a spinor representation of $O(3)$ rotations $R^{(i)}$ defined before. The detailed expressions of matrices $R^{(i)}$ and $D^{(i)}$ are given in the Appendix. Then the spin-dependent hopping Hamiltonian is given by

$$H_{L,R} = \sum_{l\sigma, l'\sigma'} \eta_{L,l\sigma}^\dagger \tilde{T}_{l\sigma, l'\sigma'} \eta_{R,l'\sigma'} + \text{H.c.}, \tag{9}$$

where

$$\tilde{T}_{l\sigma, l'\sigma'} = \frac{1}{2}[T_{\text{hop}} V_L V_R^\dagger + V_L V_R^\dagger T_{\text{hop}}]_{l,l'}[(D^{(L)})^\dagger D^{(R)}]_{\sigma,\sigma'}. \tag{10}$$

Here l is the index for d orbitals under the local trigonal crystal field ($l=a$, e_+, and e_-) and σ indicates the spin projection with respect to a local quantization axis.

We can obtain the final expression for the effective hopping Hamiltonian by introducing a matrix A which changes the trigonal basis to the local spin-orbit basis in the following way, $|\alpha\rangle = d_\alpha^\dagger|0\rangle \equiv \Sigma_{l\sigma} A_{\alpha,l\sigma} \eta_{l\sigma}^\dagger|0\rangle$. Here we denote the local spin-orbit basis using an index α ($\alpha=1,\ldots,6$). $\alpha=1,2$ indicate the spin-orbit doublet with the total angular momentum $j_{\text{eff}}=1/2$ and $\alpha=3,4,5,6$ denote the spin-orbit quadruplet with $j_{\text{eff}}=3/2$. It is straightforward to extend the approach described above for a three-site cluster to the full pyrochlore lattice system. The resulting effective lattice hopping Hamiltonian is given by

$$H_{\text{eff}} = \sum_{\langle ij \rangle} \sum_{n,n'} \sum_{\alpha,\alpha'} d_{in\alpha}^\dagger T_{n\alpha, n'\alpha'} d_{jn'\alpha'} + \text{H.c.}, \tag{11}$$

where

$$T_{n\alpha, n'\alpha'} = \sum_{l\sigma, l'\sigma'} (A^*)_{\alpha, l\sigma} \tilde{T}_{nl\sigma, n'l'\sigma'} (A^T)_{l'\sigma', \alpha'}. \tag{12}$$
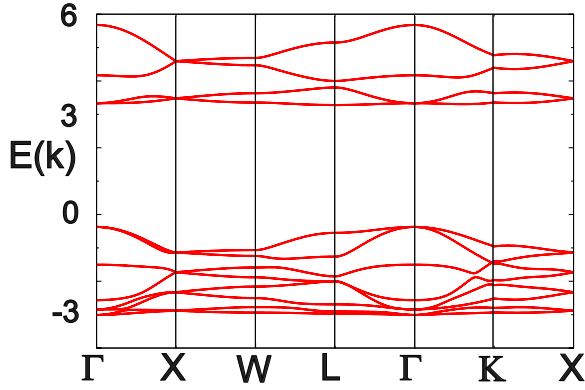
FIG. 4. (Color online) Tight-binding band structure of Ir $5d$ orbitals when there is no trigonal crystal-field effect. Here we have chosen $\lambda_{SO}=4.0$, $t_a=t_e=0.5$. Note that the upper four bands corresponding to the spin-orbit doublet ($j_{eff}=1/2$) are well separated from the other eight bands which come from the spin-orbit quadruplet ($j_{eff}=3/2$).

Here i is the unit-cell index and the index n refers to the four Ir sites within a single tetrahedral unit cell. Including the on-site potentials for the local spin-orbit eigenstates, the expression for the effective tight-binding Hamiltonian is finally given by Eq. (3).

III. EVOLUTION OF THE ELECTRONIC STRUCTURE UNDER TRIGONAL CRYSTAL FIELD

In this section, we discuss the evolution of the electronic structure of the Ir $5d$ system on the pyrochlore lattice in the presence of the trigonal crystal field. We start with the case where the Ir ions are under the perfect cubic crystal field with large spin-orbit coupling. In Fig. 4, we plot the electron band dispersion along the high symmetry directions in the Brillouin zone for the perfect cubic crystal field on the Ir ions with $\lambda_{SO}=4.0$, $t_a=t_e=0.5$. Since we have four sites within a unit cell and each site supports three t_{2g} orbitals, there are 24 bands within the first Brillouin zone including spin degrees of freedom. Due to the time-reversal and inversion symmetries, each band is doubly degenerate. In Fig. 4, the upper four bands are derived from the spin-orbit doublets with total angular momentum $j_{eff}=1/2$. On the other hand, the lower eight bands come from the quadruplets with $j_{eff}=3/2$. Note that these two groups of bands are well separated by a large energy gap with an energy scale given by λ_{SO}.

Since each Ir atom contributes five electrons, 20 bands among the 24 bands are filled. Namely, we have a band insulator with the half-filled $j_{eff}=1/2$ bands. Therefore in the forthcoming discussion, we neglect the fully occupied $j_{eff}=3/2$ bands and focus on the properties of the upper four bands (or eight bands counting the double degeneracy of each band) possessing $j_{eff}=1/2$ character. The energy dispersions of the $j_{eff}=1/2$ states are shown in Fig. 5(a). The fully occupied lower two bands are separated from the upper two bands by a finite gap between them.
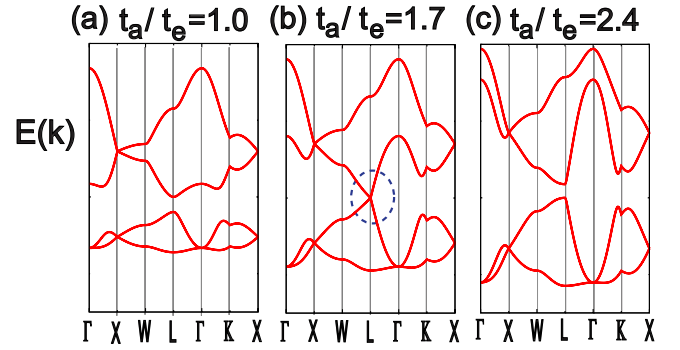

FIG. 5. (Color online) Dispersions of $j_{eff}=1/2$ bands under trigonal crystal field with $t_a>t_e$. Here we have fixed $\lambda_{SO}=4.0$, $t_e=0.5$ while changing t_a. There is an accidental band touching between the two bands in the middle at the L point when $t_a/t_e=1.7$.

To understand the topological properties of the insulating phase, we compute the Z_2 topological invariants ($\nu; \nu_1\nu_2\nu_3$) from the parity eigenvalues $\xi_m(\Gamma_l)$ at the time-reversal invariant momenta, following Fu and Kane.[9] Here $\xi_m(\Gamma_l)$ indicates the inversion parity of the mth occupied $j_{eff}=1/2$ band at the time-reversal invariant momentum Γ_l. Using the reciprocal-lattice vectors $G_i(i=1,2,3)$, the eight time-reversal invariant momenta can be written as $\Gamma_{l=n_1n_2n_3}=(n_1G_1+n_2G_2+n_3G_3)/2$ with $n_{1,2,3}=0,1$. The strong Z_2 topological invariant ν is given by

$$(-1)^\nu = \prod_{n_i=0,1} \prod_{m=1}^{2} \xi_m(\Gamma_{n_1n_2n_3}), \qquad (13)$$

where the parity eigenvalues at the eight time-reversal invariant momenta are multiplied at the same time. On the other hand, each of the three weak Z_2 topological invariants $\nu_i(i=1,2,3)$ is determined by the parity eigenvalues at the four time-reversal invariant momenta lying on a plane, which is given by

$$(-1)^{\nu_i} = \prod_{n_i=1,n_{j\neq i}=0,1} \prod_{m=1}^{2} \xi_m(\Gamma_{n_1n_2n_3}). \qquad (14)$$

Because of the time-reversal symmetry, each band is doubly degenerate at the time-reversal invariant momentum and every Kramers doublet share the same inversion parity. Since the Z_2 topological invariants count the parity of one state for each Kramers pair,[9] we consider the product of the inversion parities corresponding to the two occupied $j_{eff}=1/2$ bands in Eqs. (13) and (14). Notice that, since the product of the inversion parities of the occupied $j_{eff}=3/2$ bands is $+1$ in every time-reversal invariant momentum, we can neglect the contributions from the $j_{eff}=3/2$ bands. These analyses lead to a strong topological insulator with the Z_2 invariants (1;000) as found earlier by Pesin and Balents.[20] It is interesting to note that a strong topological insulator with the same Z_2 invariant (1;000) was also found in a simple one-band model on the pyrochlore lattice.[42]

Now we describe the effect of the trigonal crystal field on the electronic structure of the $j_{eff}=1/2$ bands. As mentioned above, the trigonal crystal-field effect can be described by

TABLE I. Inversion parities of the $j_{\text{eff}}=1/2$ bands at time-reversal invariant momenta for $\lambda_{SO}=4.0$, $t_a=t_e=0.5$. Here $E_1 \leq E_2 \leq E_3 \leq E_4$. At the momentum $X_i(i=1,2,3)$, the upper (lower) two bands are degenerate with opposite inversion parities satisfying $\epsilon \bar{\epsilon} = -1$ ($\epsilon' \bar{\epsilon}' = -1$).

|	E_1	E_2	E_3	E_4
$\Gamma(0,0,0)$	$+$	$+$	$+$	$+$
$L_0(\pi,\pi,\pi)$	$-$	$-$	$+$	$-$
$L_1(-\pi,\pi,\pi)$	$+$	$+$	$-$	$+$
$L_2(\pi,-\pi,\pi)$	$+$	$+$	$-$	$+$
$L_3(\pi,\pi,-\pi)$	$+$	$+$	$-$	$+$
$X_1(2\pi,0,0)$	ϵ	$\bar{\epsilon}$	ϵ'	$\bar{\epsilon}'$
$X_2(0,2\pi,0)$	ϵ	$\bar{\epsilon}$	ϵ'	$\bar{\epsilon}'$
$X_3(0,0,2\pi)$	ϵ	$\bar{\epsilon}$	ϵ'	$\bar{\epsilon}'$

FIG. 6. (Color online) Dispersions of $j_{\text{eff}}=1/2$ bands under trigonal crystal field with $t_a < t_e$. Here we have fixed $\lambda_{SO}=4.0$, $t_a =0.5$ but vary t_e. As t_e/t_a increases the energy gap between the two bands in the middle reduces. When $t_e/t_a \approx 2.3$ band inversion occurs at the Γ point and the system becomes metallic.

changing the relative magnitude of t_a and t_e. In general, the pyrochlore oxides have oxygen x parameters ranging from 0.309 to 0.355.[40] Since $x_c=0.3125$ for the perfect cubic crystal field, we have to consider both trigonal compression ($x > x_c$) and elongation ($x < x_c$) cases. According to the naive crystal-field splitting picture, the on-site energies E_a and E_e of a_{1g} and e'_g states are determined by the magnitude of oxygen x parameters. However, in real materials, the relative magnitude between E_a and E_e are strongly affected by hybridization with high energy e_g orbital states, which are allowed under the trigonal crystal field.[43] Therefore, irrespective of the magnitude of the oxygen x parameter, we have to investigate both $t_a/t_e > 1$ and $t_e/t_a > 1$ cases on equal footing.

We first consider the case of $t_a/t_e > 1$. In Fig. 5, we plot the evolution of the band structure as we increase t_a/t_e. For $t_a/t_e \approx 1.7$, an accidental band touching occurs at the L point in the Brillouin zone. Since the two bands touching at the L point have opposite inversion parities as shown in Table I, the band crossing induces the exchange of the parities between the two bands touching at the L point. However, since we have eight different momentum points within the first Brillouin zone, which are symmetry equivalent to the L point, the product of the inversion parities for all occupied bands is invariant. According to Fu and Kane,[9] the product of the inversion parities of occupied bands determines the Z_2 topological invariant ν, characterizing the topological properties of insulators. Therefore, the accidental band touching does not induce the change in the topological properties of the insulating states.

Now we consider the opposite limit of $t_e/t_a > 1$. Figure 6 shows the evolution of the band structure as we increase t_e/t_a. Notice that the band gap at the Γ point reduces progressively as t_e/t_a increases. In particular, when $t_e/t_a = (t_e/t_a)_c=2.3$, a band inversion occurs at the Γ point and the system becomes metallic. The double degeneracy at the Γ point is protected by the lattice point-group symmetry. Therefore the metallic phase is stable as long as symmetry breaking fields reducing the lattice symmetry are not introduced. It is interesting that a similar metallic state is
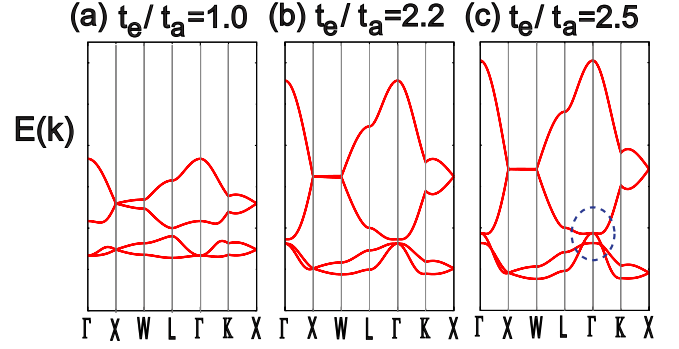
predicted by a recent first-principles calculation on $Y_2Ir_2O_7$.[44] Although we have used a simplified tight-binding approach, the overall band structure and degeneracies at the Γ point for the metallic phase are consistent with the prediction of the local-density approximation (LDA) calculation.

The effect of the trigonal crystal fields on the electronic structure is summarized in the phase diagram shown in Fig. 7. The strong topological insulator (STI) is stable against the trigonal crystal-field effect for t_e/t_a smaller than the critical value, $(t_e/t_a)_c$. On the other hand, if t_e/t_a is larger than the critical value, a metallic phase occurs. The metallic phase is stable as long as the point-group symmetry of the lattice is protected.

IV. LATTICE DISTORTION AND METAL-INSULATOR TRANSITION

In this section we study the fate of the metallic phase predicted above against external perturbations. Some pyrochlore iridates $A_2Ir_2O_7$ with A=Nd, Sm, and Eu, show metal-insulator transitions as the temperature decreases.[35,36] However, the nature of the insulating ground state is under controversy. According to a recent Raman-scattering measurement on these iridium compounds,[38] metal-insulator transitions accompany structural distortions for $Sm_2Ir_2O_7$ and $Eu_2Ir_2O_7$. In addition, a recent theoretical study on a toy
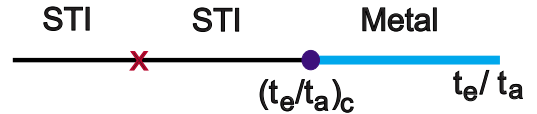

FIG. 7. (Color online) Phase diagram as a function of the strength of the local trigonal crystal field represented by t_e/t_a. Note that a metallic phase occurs when t_e/t_a becomes larger than the critical value of $(t_e/t_a)_c > 1$. The red cross in the middle of two strong topological insulators (STI) indicates the point where accidental band touching occurs.

model for the topological insulators on the pyrochlore lattice,[42] has shown that the lattice distortions along the [111] direction may be important for the realization of the topological insulator. Here we investigate the effect of lattice distortions on the fate of the metallic state. In particular, to make predictions relevant to future high-pressure experiments, we focus on uniform lattice modulations via $\mathbf{q}=0$ phonon mode softening, which lead to macroscopic volume change in the system.

Since we have four Ir ions within a tetrahedral unit cell, displacements of four Ir atoms from their equilibrium positions, $\delta\mathbf{r}_i=(\delta x_i, \delta y_i, \delta z_i)$, give rise to 12 independent degrees of freedom. Among these 12 different modes, we neglect six modes describing global translations and rotations of the unit cell, because these do not lead to distortions of the tetrahedron. The remaining six modes are classified as A_1 singlet Q^A, E doublet $\mathbf{Q}^E=(Q_1^E, Q_2^E)$, and T_2 triplet $\mathbf{Q}^T=(Q_1^T, Q_2^T, Q_3^T)$, in terms of irreducible representations for the T_d point group of the tetrahedron.[45–47] The expressions for normal coordinates Q corresponding to each irreducible representation are given by

$$Q^A = \frac{1}{\sqrt{6}}(\delta r_{14} + \delta r_{23} + \delta r_{24} + \delta r_{13} + \delta r_{34} + \delta r_{12}),$$

$$Q_1^E = \frac{1}{\sqrt{12}}(\delta r_{14} + \delta r_{23} + \delta r_{24} + \delta r_{13} - 2\delta r_{34} - 2\delta r_{12}),$$

$$Q_2^E = \frac{1}{2}(-\delta r_{14} - \delta r_{23} + \delta r_{24} + \delta r_{13}),$$

$$Q_1^T = \frac{1}{\sqrt{2}}(\delta r_{14} - \delta r_{23}),$$

$$Q_2^T = \frac{1}{\sqrt{2}}(\delta r_{24} - \delta r_{13}),$$

$$Q_3^T = \frac{1}{\sqrt{2}}(\delta r_{34} - \delta r_{12}). \tag{15}$$

In the above δr_{ij} indicates the change in the distance between the ith and jth Ir atoms. Since the Q^A mode describes a uniform elongation or contraction of all bond lengths, it does not change the symmetry of the unit cell. So we neglect the Q_A mode in the following discussion. On the other hand, the two components of the doublet $\mathbf{Q}^E=(Q_1^E, Q_2^E)$ describe tetragonal and orthorhombic distortions, respectively. Finally, each component of the triplet mode, Q_i^T depicts elongation and contraction of a pair of orthogonal bonds which are lying on two parallel planes of a cube [see Fig. 1(b)]. Equal amplitude superposition of three components of the triplet mode leads to a trigonal distortion of a tetrahedron along [111] or its equivalent directions.

Using the information about the phonon modes of a single tetrahedron, we consider various $\mathbf{q}=0$ phonon modes on the pyrochlore lattice system. The pyrochlore lattice consists of two inequivalent tetrahedra sharing a corner and these two
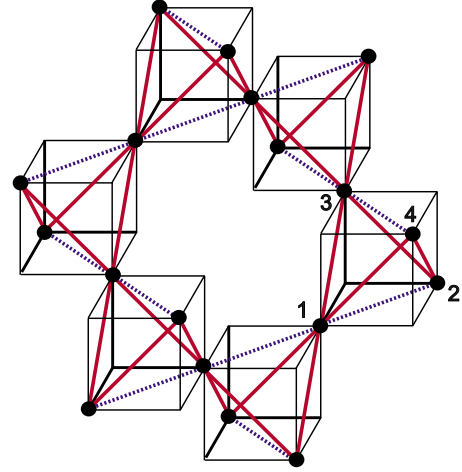

FIG. 8. (Color online) Tetragonal lattice distortion induced by a $\mathbf{q}=0$ phonon mode with E_g symmetry. Red solid and blue broken lines describe two inequivalent bond lengths under the lattice distortion.

types of tetrahedra are interchanged via inversion symmetry with respect to a corner. Therefore even when we are restricted to $\mathbf{q}=0$ phonon modes, there are lattice distortions with even and odd symmetries with respect to an inversion center. However, in this work, we focus on phonon modes with even inversion parities. This is because only the phonon modes with even parities lead to macroscopic distortion of the lattice. Therefore these modes can be softened via coupling to applied external pressure, which can be performed in future high-pressure experiments. In particular, we focus on tetragonal and orthorhombic distortions induced by E_g phonon modes and trigonal distortions driven by T_{2g} phonon modes. Structures of distorted lattices and modulations in bond lengths are described in Figs. 8 and 9.
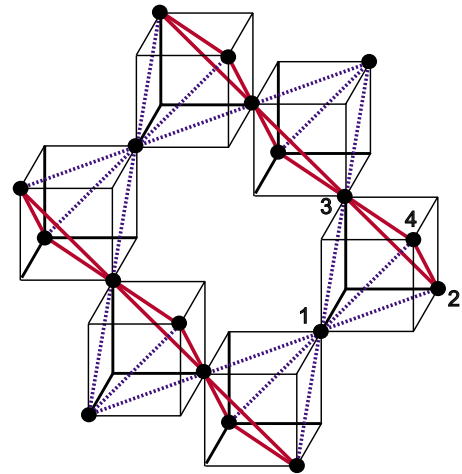

FIG. 9. (Color online) Trigonal lattice distortion induced by a $\mathbf{q}=0$ phonon mode with T_{2g} symmetry. Red solid and blue broken lines describe two inequivalent bond lengths under the lattice distortion.
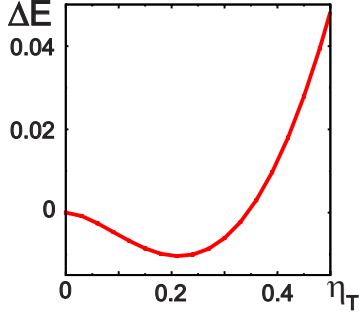
FIG. 10. (Color online) Ground-state energy per unit cell for the pyrochlore iridate system coupled with a trigonal phonon mode along [111] direction. Here $\lambda_{SO}=4.0$, $t_a=0.5$, and $t_e/t_a=2.5$. We plot the change in the ground-state energy induced by the trigonal lattice distortion as a function of the hopping amplitude modulation η_T.

Modulation of interatomic distances between neighboring Ir atoms results in the renormalization of the nearest-neighbor hopping amplitudes. To understand the effect of electron-phonon coupling on the ground-state properties of the system, we consider a Hamiltonian given by

$$H_{\text{el-ph}} = \sum_{i,n,\alpha} (\varepsilon_\alpha - \mu) d^\dagger_{in\alpha} d_{in\alpha} + \frac{1}{2}\sum_i \sum_{n,m} K_{n,m}\eta^2_{n,m}$$
$$+ \sum_{\langle ij \rangle} \sum_{n,n'} \sum_{\alpha,\alpha'} d^\dagger_{in\alpha} T_{n\alpha,n'\alpha'}(\{\eta_{n,n'}\}) d_{jn'\alpha'} + \text{H.c.},$$

$$(16)$$

where $\eta_{n,n'}$ indicates modulation of the hopping amplitude between neighboring nth and n'th Ir atoms. Specifically, we assume that $T_{n\alpha,n'\alpha'}(\{\eta_{n,n'}\})=T_{n\alpha,n'\alpha'}(\{\eta_{n,n'}=0\})(1-\eta_{n,n'})$. This is equivalent to scaling of t_a and t_e to $t_a(1-\eta_{n,n'})$ and $t_e(1-\eta_{n,n'})$ between neighboring sites n and n' [see Eqs. (10) and (12)]. Since $t_a \propto t_e \propto \alpha^2_{pd\pi}$, this approximation captures the change in the overlap integral between neighboring d and p orbitals caused by electron-phonon coupling. The elastic constant, $K_{n,n'}$, corresponding to the modulation $\eta_{n,n'}$, is simply taken to be $K_{n,n'}=1.7t_a$.

In Fig. 10 we plot the ground-state energy of the coupled electron-phonon system [Eq. (16)] as we increase the magnitude of hopping amplitude modulation η_T, which corresponds to a trigonal lattice distortion. Here $\eta_T>0$ means that the hopping amplitudes along the bonds connected with the site 1 (the broken lines in Fig. 9) are reduced by η_T while the hopping amplitudes along all other bonds are increased by the same amount. In Fig. 11, we plot the change in the electron band dispersion induced by a trigonal lattice distortion. The trigonal lattice distortion results in opening a full gap at the Fermi energy leading to an insulating phase. The competition between the electronic energy gain from gap opening and elastic energy cost compromises at the equilibrium bond distance. For $\lambda_{SO}=4.0$, $t_a=0.5$, and $t_e/t_a=2.5$, 10% modulation of the hopping amplitude η_T generates a band gap with magnitude of 0.22, which is about 4% of the $j_{\text{eff}}=1/2$ state
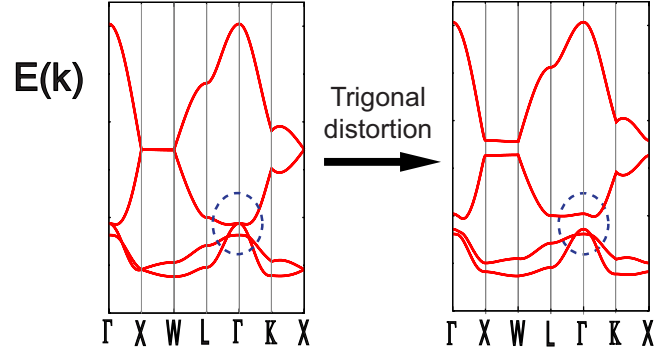

FIG. 11. (Color online) Band-structure change induced by a trigonal lattice distortion, which comes from a $\mathbf{q}=0$ T_{2g} phonon mode softening. A band gap opens at the Γ point. The resultant insulating phase is a strong topological insulator.

bandwidth. Taking into account the $j_{\text{eff}}=1/2$ state bandwidth predicted by the LDA calculation,[44] the estimated magnitude of the band gap is roughly about 40 meV. Straightforward calculation of Z_2 topological invariants shows that the resultant insulating ground state is a strong topological insulator with Z_2 invariants $(\nu;\nu_1\nu_2\nu_3)=(1;000)$. Notice that the Z_2 invariants of the new insulating phase are the same as those of the original topological insulating phase, which exists when there is no local trigonal crystal-field splitting effect.

It is interesting that two insulating phases separated by a metallic phase in between share the same topological properties. To understand the reason for the identical topological properties of two insulating phases, we have checked the inversion parities of all bands at the Γ point displayed in Table I. According to Fu and Kane,[9] for a system with time-reversal and inversion symmetries, the Z_2 topological invariants are given by the product of inversion parities of all occupied bands at time-reversal invariant momenta. As one can see in Fig. 6, the metallic phase induced by local trigonal crystal-field effect has a band crossing only at the Γ point. Since every band has even inversion parity at the Γ point, the band crossing does not change the parities of occupied bands. Therefore two insulating phases with an intervening metallic phase share the same Z_2 topological indices in this case.

In addition to trigonal lattice distortions, we have also investigated the effect of tetragonal and orthorhombic distortions, which result from softening $\mathbf{q}=0$ E_g phonon modes. The influence of various lattice distortions on the nature of the ground state is summarized in Table II. It turns out that a tetragonal distortion with $\eta_{E1}>0$ leads to an insulating ground state. Figure 8 describes a bond modulation pattern for a tetragonal distortion with $\eta_{E1}>0$. Here electron hopping amplitudes are increased for dotted bonds while the hopping amplitudes for solid bonds are reduced. Relative magnitude of bond length modulations is consistent with the Q_1^E mode, the first component of the doublet E phonon mode in Eq. (15). However, the magnitude of the band gap generated by a tetragonal distortion with $\eta_{E1}>0$ is much smaller than that from a trigonal lattice distortion when the magnitudes of hopping amplitude modulations are the same in the two cases. In addition, an orthorhombic distortion does not

TABLE II. Lattice distortions and the resulting ground states.

Lattice distortion	Ground state
Tetragonal ($\eta_{E1} > 0$)	Topological insulator
Tetragonal ($\eta_{E1} < 0$)	Metal
Orthorhombic ($\eta_{E2} > 0$)	Metal
Orthorhombic ($\eta_{E2} < 0$)	Metal
Trigonal ($\eta_T > 0$)	Topological insulator
Trigonal ($\eta_T < 0$)	Metal

open a full band gap. Therefore we propose that application of external pressure along the [111] or its equivalent directions is the most efficient way of generating strong topological insulators.

V. CONCLUSION

We investigate the possible existence of the strong topological insulators in pyrochlore iridates $A_2Ir_2O_7$. The effective Hamiltonian for the pyrochlore lattice of Ir ions is derived by taking into account the strong spin-orbit coupling and trigonal crystal-field effect. It turns out that the strong topological insulator found for the ideal cubic environment of Ir ions may turn into a metallic state under trigonal distortion of oxygen octahedra. It has been known that, in cubic pyrochlore oxides, $A_2B_2O_7$, where both A- and B-site ions reside on two distinct interpenetrating pyrochlore networks, the trigonal crystal-field splitting exists inherently[40] with an energy scale comparable to the spin-orbit coupling.[44] This may also be consistent with the recent LDA calculation of $Y_2Ir_2O_7$ where it was found that the nonmagnetic ground state would be a metal.[44,48] Given that various pyrochlore iridates with different A-site ions possess substantial but different amount of trigonal distortion, the presence of trigonal crystal-field effect may be one of the important factors that determine the nature of low-temperature ground states and finite-temperature metal-insulator transitions.

On the other hand, we found that the electron-lattice coupling also plays an important role. It is shown that certain $\mathbf{q}=0$ normal modes lead to the re-emergence of a strong topological insulator when these modes are softened and the system undergoes a structural deformation. Recent experimental observation of the pressure-induced metal-insulator transition in $Ba_{1-x}R_xIrO_3$ ($R=Gd, Eu$) suggests that electron-lattice coupling strongly affects the ground-state properties in iridium oxide compounds. Due to the sensitive response of the electronic structure near the Fermi level against the variation in Ir-O-Ir bond angles, the application of moderate hydrostatic pressure around 12 kbar destabilizes the metallic ground state leading to metal-insulator transition.[49] While the identification of the true ground state in the pyrochlore iridates would require better understanding of the electron correlation effect, it is an intriguing possibility that the strong topological insulators may arise via a finite-temperature metal-insulator transition with structural changes. Our study also suggests that the application of the external pressure along [111] or its equivalent directions may lead to a strong topological insulator by taking the advantage of the electron-lattice coupling or perhaps even to a topological Mott insulator in stronger correlation regime.

In the current work, we did not study the electron-electron interaction effect. It is possible that sufficiently strong electron interaction would turn the metallic state induced by the trigonal crystal-field effect to a magnetically ordered insulator or a more subtle form of Mott insulator. The competition between magnetically ordered Mott insulators, topological band insulators, and topological Mott insulators in the presence of electron interaction would be an excellent topic of future studies. The understanding of the delicate interplay between the electron interaction, spin-orbit coupling, local crystal-field effect, and electron-lattice coupling would be essential for the determination of the ultimate ground states in these systems. All of these possibilities await for further experimental verifications and findings.

APPENDIX: EXPLICIT MATRIX EXPRESSIONS FOR THE EFFECTIVE HOPPING HAMILTONIAN

In this appendix, we present the expressions for various matrices used to derive the effective hopping Hamiltonian in Sec. II B. We follow the same convention taken by Pesin and Balents.[20] The matrix $R^{(i)}$ rotating the global cubic axis to the local octahedral axis for the ith Ir atom is given by

$$R^{(1)} = \begin{pmatrix} \frac{2}{3} & -\frac{1}{3} & -\frac{2}{3} \\ -\frac{1}{3} & \frac{2}{3} & -\frac{2}{3} \\ \frac{2}{3} & \frac{2}{3} & \frac{1}{3} \end{pmatrix}, \quad R^{(2)} = \begin{pmatrix} \frac{2}{3} & \frac{2}{3} & \frac{1}{3} \\ -\frac{2}{3} & \frac{1}{3} & \frac{2}{3} \\ \frac{1}{3} & -\frac{2}{3} & \frac{2}{3} \end{pmatrix},$$

$$R^{(3)} = \begin{pmatrix} \frac{1}{3} & -\frac{2}{3} & \frac{2}{3} \\ \frac{2}{3} & \frac{2}{3} & \frac{1}{3} \\ -\frac{2}{3} & \frac{1}{3} & \frac{2}{3} \end{pmatrix}, \quad R^{(4)} = \begin{pmatrix} \frac{1}{3} & -\frac{2}{3} & \frac{2}{3} \\ -\frac{2}{3} & -\frac{2}{3} & -\frac{1}{3} \\ \frac{2}{3} & -\frac{1}{3} & -\frac{2}{3} \end{pmatrix}.$$

The matrix $D^{(i)}$ corresponding to a spinor representation of $R^{(i)}$ is given by

$$D^{(1)} = \begin{pmatrix} \sqrt{\frac{2}{3}} & \frac{1-i}{\sqrt{6}} \\ -\frac{1+i}{\sqrt{6}} & \sqrt{\frac{2}{3}} \end{pmatrix}, \quad D^{(2)} = \begin{pmatrix} -\frac{2+i}{\sqrt{6}} & -\frac{i}{\sqrt{6}} \\ -\frac{i}{\sqrt{6}} & -\frac{2-i}{\sqrt{6}} \end{pmatrix},$$

$$D^{(3)} = \begin{pmatrix} \frac{2-i}{\sqrt{6}} & -\frac{1}{\sqrt{6}} \\ \frac{1}{\sqrt{6}} & \frac{2+i}{\sqrt{6}} \end{pmatrix}, \quad D^{(4)} = \begin{pmatrix} -\frac{i}{\sqrt{6}} & \frac{1-2i}{\sqrt{6}} \\ -\frac{1+2i}{\sqrt{6}} & \frac{i}{\sqrt{6}} \end{pmatrix}.$$

Finally, we show the matrix A which changes the trigonal basis to local spin-orbit eigenstates as follows:

$$A = \begin{pmatrix} 0 & 0 & 0 & 0 & \frac{n_1\omega}{3} & 0 \\ 0 & 0 & 0 & 0 & 0 & \frac{-n_1\omega}{3} \\ \frac{-n_2}{6} & 0 & \frac{-in_2\omega}{6} & 0 & 0 & 0 \\ 0 & \frac{-n_2}{3\sqrt{2}} & 0 & \frac{-in_2\omega}{3\sqrt{2}} & 0 & 0 \\ \frac{n_3}{3\sqrt{2}} & 0 & \frac{-in_3}{3\sqrt{2}} & 0 & 0 & 0 \\ 0 & \frac{n_3}{\sqrt{6}} & 0 & \frac{-in_3}{\sqrt{6}} & 0 & 0 \end{pmatrix},$$

where $\omega = e^{i(2\pi/3)}$ and $[n_1 n_2 n_3]$ indicates the local C_3 symmetry axis of the corresponding distorted oxygen octahedron.

[1] X.-L. Qi and S.-C. Zhang, Phys. Today **63**(1), 33 (2010).

[2] M. Hasan and C. L. Kane, arXiv:1002.3895 (unpublished).

[3] C. L. Kane and E. J. Mele, Phys. Rev. Lett. **95**, 146802 (2005).

[4] C. L. Kane and E. J. Mele, Phys. Rev. Lett. **95**, 226801 (2005).

[5] B. A. Bernevig, T. L. Hughes, and S.-C. Zhang, Science **314**, 1757 (2006).

[6] B. A. Bernevig and S.-C. Zhang, Phys. Rev. Lett. **96**, 106802 (2006).

[7] L. Fu, C. L. Kane, and E. J. Mele, Phys. Rev. Lett. **98**, 106803 (2007).

[8] J. E. Moore and L. Balents, Phys. Rev. B **75**, 121306(R) (2007).

[9] L. Fu and C. L. Kane, Phys. Rev. B **76**, 045302 (2007).

[10] L. Fu and C. L. Kane, Phys. Rev. B **74**, 195312 (2006).

[11] R. Roy, Phys. Rev. B **79**, 195321 (2009).

[12] R. Roy, Phys. Rev. B **79**, 195322 (2009).

[13] M. König, S. Wiedmann, C. Brune, A. Roth, H. Buhmann, L. W. Molenkamp, X.-L. Qi, and S.-C. Zhang, Science **318**, 766 (2007).

[14] D. Hsieh, D. Qian, L. Wray, Y. Xia, Y. S. Hor, R. J. Cava, and M. Z. Hasan, Nature (London) **452**, 970 (2008).

[15] Y. Xia, D. Qian, D. Hsieh, L. Wray, A. Pal, H. Lin, A. Bansil, D. Grauer, Y. S. Hor, R. J. Cava, and M. Z. Hasan, Nat. Phys. **5**, 398 (2009).

[16] H. Zhang, C.-X. Liu, X.-L. Qi, X. Dai, Z. Fang, and S.-C. Zhang, Nat. Phys. **5**, 438 (2009).

[17] D. Hsieh, Y. Xia, D. Qian, L. Wray, J. H. Dil, F. Meier, J. Osterwalder, L. Patthey, J. G. Checkelsky, N. P. Ong, A. V. Fedorov, H. Lin, A. Bansil, D. Grauer, Y. S. Hor, R. J. Cava, and M. Z. Hasan, Nature (London) **460**, 1101 (2009).

[18] Y. L. Chen, J. G. Analytis, J.-H. Chu, Z. K. Liu, S.-K. Mo, X. L. Qi, H. J. Zhang, D. H. Lu, X. Dai, Z. Fang, S. C. Zhang, I. R. Fisher, Z. Hussain, and Z.-X. Shen, Science **325**, 178 (2009).

[19] A. Shitade, H. Katsura, J. Kunes, X.-L. Qi, S.-C. Zhang, and N. Nagaosa, Phys. Rev. Lett. **102**, 256403 (2009).

[20] D. A. Pesin and L. Balents, Nat. Phys. **6**, 376 (2010).

[21] B. J. Kim, H. Jin, S. J. Moon, J.-Y. Kim, B.-G. Park, C. S. Leem, Jaejun Yu, T. W. Noh, C. Kim, S.-J. Oh, J.-H. Park, V. Durairaj, G. Cao, and E. Rotenberg, Phys. Rev. Lett. **101**, 076402 (2008).

[22] B. J. Kim, H. Ohsumi, T. Komesu, S. Sakai, T. Morita, H. Takagi, and T. Arima, Science **323**, 1329 (2009).

[23] S. J. Moon, H. Jin, W. S. Choi, J. S. Lee, S. S. A. Seo, J. Yu, G. Cao, T. W. Noh, and Y. S. Lee, Phys. Rev. B **80**, 195110 (2009).

[24] H. Jin, H. Jeong, T. Ozaki, and J. Yu, Phys. Rev. B **80**, 075112 (2009).

[25] Y. Okamoto, M. Nohara, H. Aruga-Katori, and H. Takagi, Phys. Rev. Lett. **99**, 137207 (2007).

[26] J. M. Hopkinson, S. V. Isakov, H.-Y. Kee, and Y. B. Kim, Phys. Rev. Lett. **99**, 037201 (2007).

[27] M. J. Lawler, H.-Y. Kee, Y. B. Kim, and A. Vishwanath, Phys. Rev. Lett. **100**, 227201 (2008).

[28] M. J. Lawler, A. Paramekanti, Y. B. Kim, and L. Balents, Phys. Rev. Lett. **101**, 197202 (2008).

[29] Y. Zhou, P. A. Lee, T.-K. Ng, and F.-C. Zhang, Phys. Rev. Lett. **101**, 197201 (2008).

[30] D. Podolsky and Y. B. Kim, arXiv:0909.4546 (unpublished).

[31] M. R. Norman and T. Micklitz, Phys. Rev. B **81**, 024428 (2010).

[32] G. Chen and L. Balents, Phys. Rev. B **78**, 094403 (2008).

[33] M. W. Young, S.-S. Lee, and C. Kallin, Phys. Rev. B **78**, 125316 (2008).

[34] H. Jin, H. Kim, H. Jeong, C. H. Kim, and J. Yu, arXiv:0907.0743 (unpublished).

[35] J. S. Gardner, M. J. P. Gingras, and J. E. Greedan, Rev. Mod. Phys. **82**, 53 (2010).

[36] K. Matsuhira, M. Wakeshima, R. Nakanishi, T. Yamada, A. Nakamura, W. Kawano, S. Takagi, and Y. Hinatsu, J. Phys. Soc. Jpn. **76**, 043706 (2007).

[37] D. Yanagishima and Y. Maeno, J. Phys. Soc. Jpn. **70**, 2880 (2001).

[38] T. Hasegawa, N. Ogita, K. Matsuhira, S. Takagi, M. Wakeshima, Y. Hinatsu, and M. Udagawa, J. Phys.: Conf. Ser. **200**, 012054 (2010).

[39] N. Taira, M. Wakeshima, and Y. Hinatsu, J. Phys.: Condens. Matter **13**, 5527 (2001).

[40] M. A. Subramanian, G. Aravamudan, and G. V. Subba Rao,

Prog. Solid State Chem. **15**, 55 (1983).

[41] M. Mączka, M. L. Sanjuán, A. F. Fuentes, L. Macalik, J. Hanuza, K. Matsuhira, and Z. Hiroi, Phys. Rev. B **79**, 214437 (2009).

[42] H.-M. Guo and M. Franz, Phys. Rev. Lett. **103**, 206805 (2009).

[43] S. Landron and M.-B. Lepetit, Phys. Rev. B **77**, 125106 (2008).

[44] Heungsik Kim and Jaejun Yu (unpublished).

[45] M. Tinkham, *Group Theory and Quantum Mechanics* (McGraw-Hill, New York, 1964).

[46] O. Tchernyshyov, R. Moessner, and S. L. Sondhi, Phys. Rev. B **66**, 064403 (2002).

[47] O. Tchernyshyov and G.-W. Chern, arXiv:0907.1693 (unpublished).

[48] X. Wan, J. Dong, and S. Y. Savrasov, arXiv:1003.3414 (unpublished).

[49] O. B. Korneta, S. Chikara, S. Parkin, L. E. DeLong, P. Schlottmann, and G. Cao, Phys. Rev. B **81**, 045101 (2010).